Resolving eddies by local mesh refinement

S. Danilov[*,a,b], Q. Wang[a]

[a]*Alfred Wegener Institute, Helmholtz Centre for Polar and Marine Research, 27515 Bremerhaven, Germany*
[b]*A. M. Obukhov Institute of Atmospheric Physics RAS, Moscow, Russia*

Abstract

Nesting in large-scale ocean modeling is used for local refinement to resolve eddy dynamics that would not be accessible otherwise. Unstructured meshes offer this functionality too by adjusting their resolution according to some goal function. However, by locally refining the mesh one does not necessarily achieve the goal resolution, because the eddy dynamics, in particular the ability of eddies to release the available potential energy, also depend on the dynamics on the upstream coarse mesh. It is shown through a suite of experiments with a zonally re-entrant channel that baroclinic turbulence can be out from equilibrium in wide (compared to a typical eddy size) zones downstream into the refined area. This effect depends on whether or not the coarse part is eddy resolving, being much stronger if it is not. Biharmonic viscosity scaled with the cube of grid spacing is generally sufficient to control the smoothness of solutions on the variable mesh. However, noise in the vertical velocity field may be present at locations where the mesh is varied if momentum advection is implemented in the vector invariant form. Smoothness of vertical velocity is recovered if the flux form of momentum advection is used, suggesting that the noise originates from a variant of the Hollingsworth instability.

Key words: Unstructured meshes, nesting, Hollingsworth instability

1. Introduction

Nesting is a widely used tool in studies of large-scale ocean circulation, helping to resolve eddy dynamics over a limited area. The interest to nesting is motivated by several factors. For one thing, running a global fine-resolution model can still be prohibitively expensive if one's focus is on the regional dynamics. For another, the Rossby radius of deformation is rather small at high latitudes, so that resolving eddies there may require excessively fine resolution elsewhere if the resolution is uniform. There are numerous examples in the literature showing the success of the nesting approach (see, e. g., Chanut et al. (2008), Durgadoo et al. (2013), Mertens et al. (2014)), while the general principles of two-way nesting algorithms are reviewed by Debreu and Blayo (2008).

Unstructured meshes offer geometric flexibility and freedom with respect to mesh design, and may serve as an alternative to the nesting approach for structured meshes. In addition to applications where the unstructured meshes are used

*Corresponding author.
Email address: Sergey.Danilov@awi.de (S. Danilov)

to better represent the domain geometry (see, e. g., Wekerle et al. (2013), Timmermann and Hellmer (2013)), the use of mesh refinement as a tool to resolve eddies is already a proven concept (see Ringler et al. (2013)). However, if the mesh resolution is allowed to vary, questions arise about the optimal way and consequences of varying it. Physical principles governing the selection of mesh resolution depend on applications, and not surprisingly, there is no unique solution. The review by Greenberg et al. (2007) mentions some aspects, and each real application may add new details.

We focus below only on one aspect of the problem related to the use of locally refined meshes to resolve eddying regimes. The amplitude of eddy motions simulated by a numerical model in a particular subdomain depends not only on the local resolution, but also on the presence of upstream perturbations, which serve as the seeds from which perturbations grow, and facilitate the release of available potential energy. While this remark may seem trivial, its implications can be very easily underestimated, and this study seeks to address them in a qualitative way. Although we deal with unstructured meshes, the results reported below can be of interest to a wider community of ocean modelers working with nesting tools on standard structured meshes.

We consider a baroclinically unstable eastward flow in a zonally-reentrant channel, where the baroclinicity is maintained through forcing at its southern (warming) and northern (cooling) walls. A linear equation of state is used with the temperature being the only scalar field influencing the density. The flow is simulated on triangular meshes composed of nearly equilateral triangles. The resolution varies in the zonal direction, and by observing the flow variability along the channel the effect of the change in the mesh resolution is assessed.

A remark is due from the very beginning. Although the mesh refinement is discussed, the dissipative operators are always varied accordingly, and the refinement means not only smaller scales but simultaneously smaller coefficients in explicit dissipative operators, and similar reduction in effective implicit dissipation associated with upwinding or flux limiting in transport equations. These two aspects (refinement and reduced dissipation coefficients) are inseparable, for dissipative operators are always designed to dispose of eddy variance of scalars and the eddy enstrophy on the grid scale. According to linear instability theory the wavelength of the most unstable wave (we take the Eady instability problem as an example) scales as $\lambda \approx 3.9\pi L_R$ where $L_R = NH/\pi f$ is the first internal Rossby radius, N the buoyancy frequency, f the Coriolis parameter and H the fluid thickness. On meshes called eddy-permitting (1/3-1/4° at midlatitudes), eddies with the size of $\lambda/2$ can already be well represented, and yet it is well known that this resolution is by far insufficient. The point is that the accompanying subgrid dissipation still turns out to be too high so that only a part of the extracted available potential energy (APE) is fluxed back to maintain kinetic energy at large scales, while the other part is lost to subgrid dissipation on small scales (see Jansen and Held (2014) for the spectral analysis of the APE release rate and energy transfers on eddy-permitting and resolving meshes). According to the results obtained in

Jansen and Held (2014) in simulations with a biharmonic Leith subgrid operator, the APE release rate saturates at resolutions between 2 to 3 grid intervals per L_R, which as we shall see, also agrees with this study. Note also that this correlates with the analysis of Hallberg (2013) for a related topic.

Our main goal below is to explore the response of turbulent flow to changes in mesh resolution, concentrating on the retardation and overshoots in eddy variability, and also on the ability to maintain smooth solutions in domains where resolution varies. Since mesh refinement also implies reduced dissipation and higher variability, a question on whether the dissipative operators can control the smoothness of solutions in regions where the resolution is adjusted back from fine to coarse one is tightly linked to the main goal.

2. Configuration and model

Most of the experiments are carried out in a zonally-reentrant channel L =40° long (0°E–40°E) occupying the latitude belt between 30° N and 45° N. The geometry is spherical. There are 24 unevenly distributed layers going down to 1600 m. Thiangular surface meshes of variable resolution are used. The basic coarse resolution is 1/3°, and the basic fine resolution is 1/12°, giving the mesh refinement (or stretching) factor, measured as the ratio of the largest to the smallest mesh edges, $r = 4$. Meshes are refined via relatively narrow transitional zones centered in most cases at ϕ_w=7.5°E and ϕ_e=32.5°E, so that more than a half of the domain is well resolved, and the other part is left coarse. The mesh resolution (edge length) h varies according to the hyperbolic tangent,

$$h = h_0(r + 0.5(r-1)(-\tanh((\phi-\phi_w)/w_t) + \tanh((\phi-\phi_e)/w_t))) \qquad (1)$$

where h_0 is the side of the smallest triangle, and w_t (in degrees) defines the width of the transitional zone. There are some variations of this basic setup. The parameters of the meshes used in different runs are presented in Table 1.

The density depends linearly on the temperature, $\rho - \rho_r = -\rho_r\alpha(T - T_r)$, with ρ_r and T_r the constant reference values and $\alpha = 2.5\times10^{-4}$ K^{-1} the thermal expansion coefficient. The initial temperature distribution is linear in the meridional direction with the gradient $T_{0y} = -0.5 \times 10^{-5}$ K/m and also in the vertical direction with the gradient T_{0z} =8×10^{-3} K/m in the entire channel. There are buffer zones 1.5° wide adjacent to the northern and southern walls where the temperature is relaxed to the initial one over the entire depth. The inverse relaxation time scale varies linearly from (3 day)$^{-1}$ at the wall to zero outside the 1.5° zones. A small sinusoidal perturbation is applied to the temperature to speed up the development of the baroclinic instability, which equilibrates in about half a year. We only deal with short runs of several years (4 or 5) in duration and present the results averaged over the entire period of integration excluding the first year. While this is certainly insufficient to obtain stationary patterns of eddy variances, it is sufficient to draw qualitative conclusions for our questions. The configuration is schematically presented in the top panel of Fig. 1.

run	rh_0	h_0	w_t	ϕ_w	L
A	1/3	1/12	1	7.5	40
A′	1/3	1/12	2.5	7.5	40
B	1/3	1/18	1.5	7.5	40
C	1/3	1/12	1.5	7.5	60
C′	1/3	1/12	4.5	10	60
D	1/6	1/24	1.5	7.5	40
E	1/9	1/36	1.5	10	40

Table 1: Geometrical parameters of meshes used, see Eq. (1). ϕ_e is always symmetric to ϕ_w with respect to the center of the mesh. The second and third column specify the coarse and fine resolution. All quantities are in degrees.

Runs A and A′ use the mesh refinement factor $r = 4$, and differ in the width of transitional zone $w_t = 1°$ (A) and $w_t = 2.5°$ (A′). Run B is performed on a mesh with $w_t = 1.5°$, and a resolution of 1/18° in the fine resolution domain ($r = 6$). Run C is similar to A, but the channel is longer (60°), with the same length of the coarse resolution domain, but an extended fine resolution domain. In C′ the transitional part is rather wide, and for that reason ϕ_w (ϕ_e) is moved a bit to the east (west). Case D doubles the resolution of the mesh of case A making it eddy resolving everywhere (see below), while case E improves the resolution further. In this case ϕ_w (ϕ_e) is also slightly shifted in order to make the length of the coarse part equal to the fine one (for both are eddy resolving).

The simulations are performed with a finite-volume ocean circulation model described in Danilov (2012). It uses a cell-vertex (quasi-B-grid) discretization. The runs are stabilized with a weak quadratic bottom drag (with C_d=0.001) and biharmonic viscosity. The scalar advection is simulated with a variant of a gradient reconstruction scheme which combines 3rd and 4th order estimates (weighted as 0.15/0.85), with the 3rd order part responsible for some upwind diffusion. On uniform meshes it is equivalent to a flow-oriented biharmonic operator. No explicit horizontal diffusion is used, and the Pacanowski–Philander scheme (Pacanowski and Philander (1981)) is applied for vertical mixing. The biharmonic viscosity coefficient includes contributions from the Smagorinsky, Leith and modified Leith parameterizations (see Fox-Kemper and Menemenlis (2008) for a review), multiplied with the areas of mesh cells (to 'translate' them from the original harmonic to the biharmonic form). It is capped at $A_{bh} = v_v S_c^{3/2}$, where $v_v = 0.02$ m/s and S_c is the cell area. Additionally, because of the too large velocity space of the cell-vertex discretization, we apply a background 'biharmonic' filter as detailed in Danilov and Androsov (2015). It provides an efficient coupling of velocities at the nearest cells. It is equivalent to the biharmonic viscosity operator with the coefficient $v_f h^3$, where $v_f = 0.007$ m/s, on a uniform equilateral mesh, but deviates from it on general meshes. No 'manual' tuning of dissipation is performed. The vector-invariant form of momentum advection is used in the runs listed in Table 1. It turned out that it may lead to a transient noisy pattern in the vertical velocity over the varying portion of mesh (see the next section), but it does not affect the main result here.

By construction, the vertical shear is $\Lambda = g\alpha T_{0y}/f$, which introduces the inverse time scale and, multiplied with the fluid depth, the scale for the horizontal velocity $U = \Lambda H$. There are two more inverse time scales set by the Coriolis frequency f and the buoyancy frequency $N^2 = g\alpha T_{0z}$, which together with Λ would lead to two dimensionless parameters related to the evolution of baroclinic instability.

The bottom drag (C_d) affects the vertical profile, removing the symmetry between the surface and the bottom, and thus influences the propagation speed of unstable baroclinic perturbations. The ratio between the largest (south) to smallest (north) Rossby radii is $\sqrt{2}$, so that coarse and fine meshes are either eddy permitting or eddy resolving for all latitudes, but there is no symmetry between the north and south. The strength of variability depends on the Reynolds numbers based on the scale of eddies and grid scale and on respective Peclet numbers. Variations in these parameters will lead to quantitative changes, but are not expected to change our conclusions on a qualitative level.

3. Results

3.1. Retarded turbulence development

The middle and bottom panels of Fig. 1 show a snapshot of temperature and relative vorticity at a depth of 100 m in case A, which is typical of the flow at other times. The two lines in the bottom panel are drawn at $\phi = \phi_w$ and $\phi = \phi_e$. The temperature distribution is indicative of the presence of a strong eastward flow (with zonal velocities in excess of 1 m/s). The relative vorticity pattern illustrates the marked difference in eddy dynamics on the coarse and fine parts of the mesh and between the upstream and downstream parts of the refined domain. Indeed, eddies do not appear immediately as the mesh is refined, but develop downstream of the western edge of the fine-resolution section. The estimate $1/\tau \sim 0.3\Lambda f/N$ for the maximum growth rate of linear Eady instability problem gives for the turbulence development length $L \sim U\tau \sim 3\pi L_R$, which is approximately just the scale of the fastest growing waves (in this estimate U should be the amplitude of velocity at steering level, which is about half of the surface velocity, but we neglect this difference). For the linear stratification used by us, $N = 4.5 \times 10^{-3}\ \mathrm{s}^{-1}$, resulting in $L_R \approx 26$ km at the channel axis, and L about 3°. The cyclones forming around the longitude of 10° have the size of $L/2$, in agreement with this scaling. A much longer distance is needed for turbulence to equilibrate downstream, through the formation of new eddies and their straining into elongated vorticity filaments.

In order to see the turbulence 'retardation' effect, we present the pattern of the standard deviation (std) of the sea surface height (ssh) in Fig. 2. While longer time averaging is needed to make the pattern more uniform, we can nevertheless conclude that the turbulence is suppressed for about 8-10° into the refined domain, but overshoots past the downstream edge of the refined area. Here we measure the 'retardation' length as the distance where the std is still less than the median value between the coarse-mesh and fine-mesh values. The extent of suppression

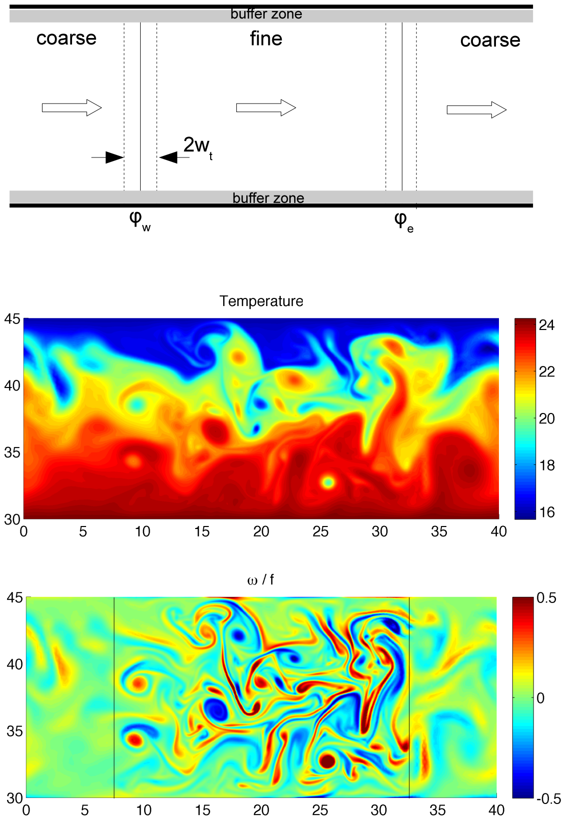

Figure 1: Top: Setup schematics. Large arrows indicate the flow direction. The solid meridional lines show the centers of transitional zones, the dashed lines mark the transitional zones, as described by Eq. (1). Middle and bottom: Snapshots of temperature (°C) and relative vorticity (normalized by the local value of the Coriolis parameter) at approximately 100 m depth in case A. While only the sharpness of temperature filaments reveals the presence of mesh refinement in the middle panel, the relative vorticity field shows the formation of eddies on the fine mesh and their decay on the coarse mesh.

or overshoot depends on the quantity being explored. In a quasi-geostrophic scaling the spatial spectrum of elevation variance will be dominated by larger scales compared to the spectra of horizontal velocity or relative vorticity. This implies that the difference between the eddy-permitting (coarse) and eddy resolving (fine) parts of the mesh is less expressed in the ssh variability, and it is only a factor of about 2 in Fig. 2.

The variability of other fields, likewise, confirms the presence of 'retardation'. We use the meridionally averaged variance of three-dimensional fields to further demonstrate it. Figure 3 shows, from top to bottom, the mesh resolution h/h_0 as given by Eq. (1) (1 corresponds to 1/12°), std for temperature, relative vorticity and vertical velocity, and the pattern of the eddy kinetic energy. All patterns of variability convey the same message and show, similar to Fig. 2 above, that the turbulence saturation is delayed some distance downstream into the refined domain. Note that the colorbar does not drop to zero for the temperature variability, and consistent with the behavior of the ssh, the std of temperature varies only within a factor of 2. Clearly, this ratio would be larger if the coarse mesh were coarser. The changes seen in the vertical velocity and relative vorticity are more dramatic. The new aspect of patterns in Fig. 3 (compared to Fig. 2) is the modulation of variability with depth showing that the turbulent flow did not reach a fully saturated level even at the end of the refined zone. The variability gradually propagates into deeper layer, a process continuing downstream to longitude of about 30°, although this adjustment is not as strong as the change at the leading part of the refined domain.

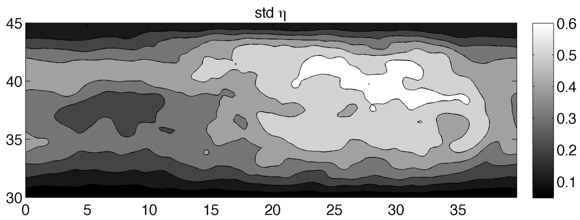

Figure 2: Standard deviation of sea surface height (m) in case A (contours are drawn in 0.1 m intervals). The centers of transitional zones are at 7.5 and 32.5°. The 'quasi-equilibrium' behavior is only reached 8-10° downstream into the refined domain, beginning from the longitude of 18-20°. In contrast, the variability is stronger than would be maintained on the coarse mesh for about 5° downstream the fine-coarse transition.

As the mesh becomes coarser (past 32.5°), the turbulence decays. Among the fields shown in Fig. 3, the temperature variability survives the furthest. The relative vorticity variability drops down almost within the mesh transition zone. This is linked to the fact that the relative vorticity variance is contributed by the smaller scales of the flow compared to the temperature or velocity.

The amount of the available potential energy released by eddies depends on their strength, so that the patterns presented above should correlate with the pattern of the conversion rate of the available potential energy to the kinetic energy. In Fig. 4 we present the time and meridional mean of the distribution of the conversion rate $R = -g\rho w$, where ρ is the density perturbation and w the vertical velocity, in run A[1]. The temperature relaxation zones adjacent to the walls are excluded from averaging, so the quantity shown is mostly contributed by eddy perturbations. The distribution of R as a function of horizontal coordinate remains patchy for the available duration of experiments, but reveals a consistent pattern after meridional averaging. The negative contributions in Fig. 4 originate from the vicinity of the southern wall. The modulation seen in the pattern is linked to the lack of zonal symmetry in the variability, as suggested by the asymmetry between the northern and southern part of the channel in Fig. 2 (the mean flow also contains a non-zonal pattern). Despite the modulation, the coarse part of the

[1]Note that the released energy is redistributed, so it does not coincide with the pattern of pressure work.

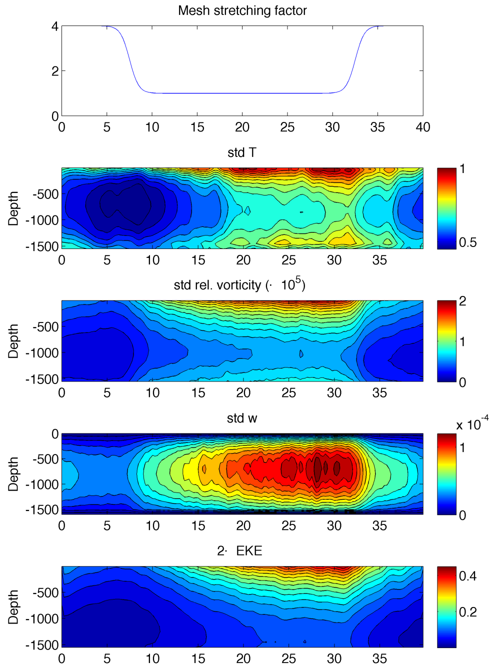

Figure 3: Mesh stretching factor (top) and the meridional mean patterns of standard deviation for temperature (°K), relative vorticity (s^{-1}), vertical velocity (m/s) and eddy kinetic energy (m^2/s^2) in case A.

channel and the initial part of the fine mesh are characterized by lower values of R, and the areas of increased R gradually go deeper until 15° E.

3.2. Smooth versus sharp mesh transitions and further mesh refinement

Case A′ and case B show very similar behavior to case A and are not displayed. For A′ the underlying reason is rather simple. The resolution of 1/3° is still coarse ($h \sim L_R$) and supports only weak transient motions for the selected viscosity in the flow entering the fine-resolution part. So as far as the geometrical transition zone remains narrower than the physical transition zone needed for the turbulent flow to saturate, its width is of little relevance (but see further). Case B is characterized by the finer resolution and hence smaller dissipation. One might expect that the turbulent flow will evolve faster into a saturated regime, which is, however, not observed. This signals that the subgrid dissipation on the 1/12° mesh of case A is already sufficiently small, so that further refinement and decrease in viscosity and implicit diffusivity only leads to the formation of smaller scales leaving the larger-scale part of the spectrum unmodified. Understanding all the detail requires a separate study, which is not pursued here. Although we have not performed runs with even larger refinement factors, we would expect that the same 'retarded' behavior will be observed even then.

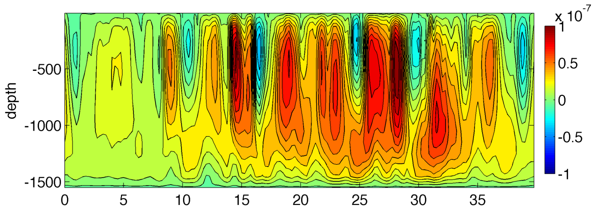

Figure 4: The meridionally averaged distribution of the APE conversion rate (in W/m^3) in case A. The narrow forcing bands in the vicinity of the northern and southern walls are excluded. The black areas correspond to the negative conversion rate, and it is positive outside them. The alternating character of the distribution is linked to the presence of non-zonal component in the mean flow caused by the change in mesh resolution.

Since the length of the fine part in case A seems to be insufficient for reaching full equilibration, simulations have been repeated on a mesh with the fine part approximately twice as long (C and C′). The temperature variability in case C, as shown in Fig. 5, is close to equilibrium east of 33°, indicating that the channel of cases A and B is indeed too short. For the longer channel, according to the pattern of temperature variability, the initial evolution of turbulence (between 10°–17°) is followed by the region between the longitudes of 17° and 33° where the strength of turbulence is still under adjustment, although at a slower rate. It is close to equilibrium on the remaining part of the fine mesh. Similar behavior is seen for the vertical velocity, relative vorticity and kinetic energy, yet it is also clear that full equilibrium is not reached even in the long channel. The variability of relative vorticity and the eddy kinetic energy continue to propagate to deeper layers all the way to ϕ_e. In order to characterize this behavior, in Fig. 6 we present the std of relative vorticity (thick black curve) averaged both meridionally and vertically. The thin black curve represents an exponential fit, $F(x) = a + b\exp(-(x-\phi_w)/L_s)$, with the e-folding length L_s=10°, and parameters a and b set by the std values at $x = \phi_w$ and the end of the fine mesh section. We will refer to L_s further as the saturation length. Fitting the variability of other fields suggests L_s between 10 and 13°.

Working with the longer channel gives us the possibility to explore the effect of very gradual transition in mesh resolution. The right panel in Fig. 5 shows the statistics for case C′ in which the transitional zones are approximately of the length of the coarse part of the channel, and are also comparable to the distance it takes to reach saturation in cases A and C. Although there are some differences, the central, equilibrated parts between 25° and 45°, where the resolution is fine on both meshes, are rather similar. For the 'coarse-fine' transition an offset to the east is observed in patterns of relative vorticity and kinetic energy in case C′, which is explained by the larger ϕ_w (see Table 1). The decay becomes more gradual on the 'fine-coarse' transition in case C′. We therefore conclude that smooth transition does not hinder reaching the equilibrium even for transition zones comparable in size to the physical length needed to reach saturation in cases A and C. To facilitate the comparison, Fig. 6 presents also the meridionally and vertically mean std of

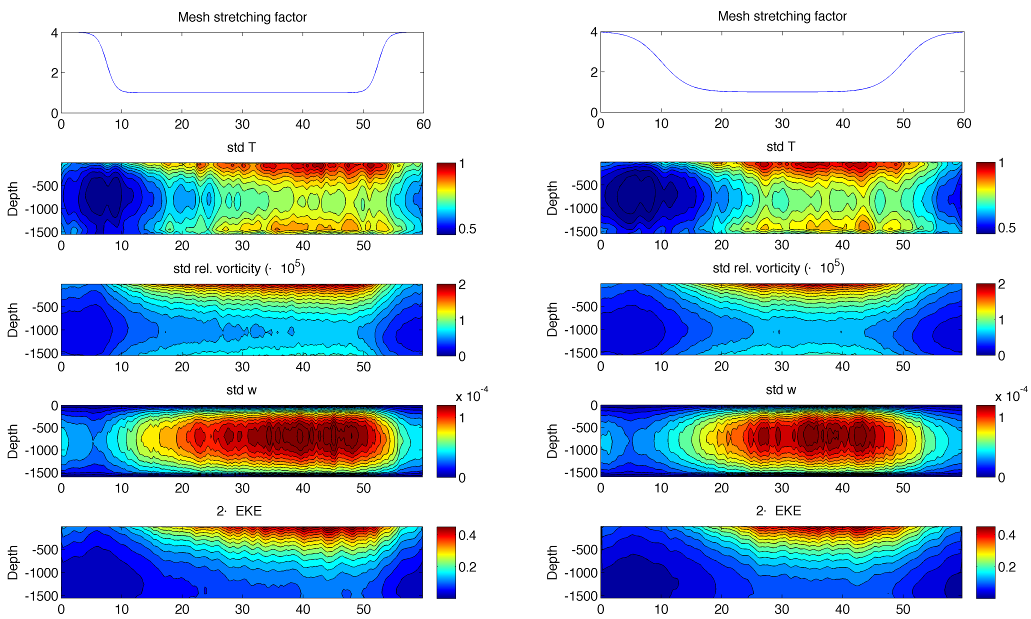

Figure 5: Left: Same as in Fig. 3, but in a longer channel (case C). Right: Case C′ where the transition between coarse and fine mesh is made more gradual.

relative vorticity in run C′ (thick gray curve), with the exponential fit based on L_s found for case C. There is a clear offset of 2.5° between the black and gray curves on the west of the refined mesh, but both approach their quasi-equilibrium further downstream approximately by the same exponential law despite the resolution is coarser in case C′ over a distance of about L_s.

In practice one would like to reach a goal resolution in a predefined domain, and the question is how this resolution has to be matched to the coarse one outside. The comparison presented in Fig. 5 and 6 can be viewed from this perspective. Let us arbitrarily define the boundary of the refined domain to be where $r = 1.1$, which is at approximately 9.2° E for case C and 17.6° E for case C′ on the west side (indicated by arrows in Fig. 6). Considering the longitude of 25° as the place where the turbulence becomes saturated in both cases, we see that in case C′ one would sacrifice less of the fine-resolution domain than in case C. Viewed from this standpoint, smooth transitions should be preferred, and the size of the transitional zone should be comparable to the length needed for turbulence to saturate. In designing a mesh, the transition zone should start sufficiently far outside the region of interest. This length may also depend on the resolution of the coarse part of the mesh.

One does not expect large changes to the behavior presented above if the coarse mesh is made even coarser except for even further suppressed variability over the coarse part of the domain and perhaps somewhat longer equilibration zone. Indeed, the transient features that serve as seeds for the baroclinic instability over the fine

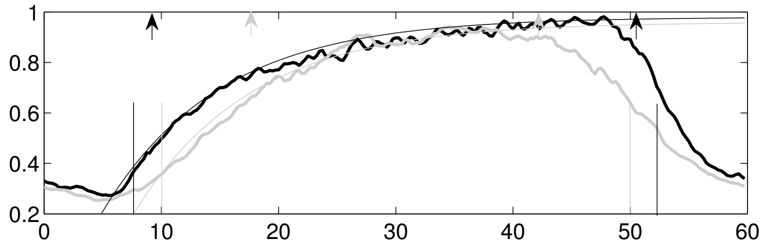

Figure 6: The std of relative vorticity averaged meridionally and vertically, in 10^{-5} s^{-1}, in cases C (thick black curve) and C′ (thick gray curve). Thin lines correspond to exponential fit with the e-folding (saturation) scale $L_s = 10°$. The vertical thin lines indicate positions of the centers of the mesh transition zones. The arrows show the boundaries of fine mesh where $r = 1.1$.

mesh are already not strong enough on the eddy-permitting coarse mesh in cases A-C, so that further coarsening would not change the overall picture. In contrast, refining the coarse mesh so that it becomes eddy resolving may have an impact on the turbulence 'retardation', as indicated by the results of cases D and E shown in Fig. 7. Note that the transition zones are centered at 10° and 30° in case E so that the fine part occupies exactly a half of the channel.

In case D the mesh is twice as fine as in case A, so that the Rossby radius L_R is approximately resolved by two triangles on the coarse mesh. While some delay in reaching saturation downstream the 'coarse-fine' transition zone is still present, the temperature and relative vorticity patterns now change much more sharply (much smaller distance is needed to reach saturation) than in case A. There is much more uniformity in the patterns of vertical velocity and EKE.

In case E the mesh is further refined, and now the coarse mesh resolution approximately corresponds to three elements per the Rossby radius. At this resolution, there is little difference in the variability of temperature and eddy kinetic energy between the coarse and fine parts of the mesh, but there are still differences in the relative vorticity and vertical velocity fields. These fields are contributed by small scales of the flow, so they show less saturation than the variability of temperature and velocity as the mesh is refined. The 'coarse-fine' transition is now sharp for all fields, with no apparent 'retardation' (there is still some delay in case D). We conclude that the resolution of about two mesh elements per Rossby radius is critical for representing eddies, similar to the conclusion in Hallberg (2013). At finer resolution the large-scale part of the flow is already faithfully modeled, and we may guess that the APE to KE conversion is close to saturation everywhere in the domain.

3.3. Vertical velocity in transitional zones

Thus far we have dealt with the retardation of the turbulence development related to the lack of sufficiently strong perturbations in the flow upstream of the fine-resolution area. We concluded that smooth transition should be preferred. We discuss now some numerical aspects related to the variable resolution as applied

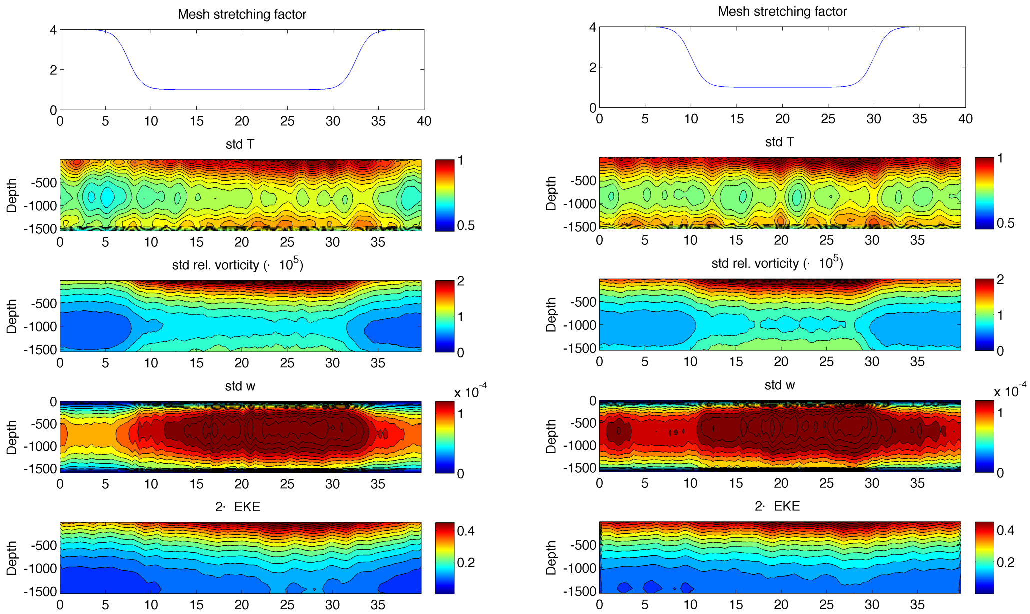

Figure 7: Same as in Fig. 3, but on a finer mesh, for case D (left) and case E (right). In both cases the ‘coarse’ part is eddy-resolving. In case E the fine part is slightly shorter than in case D, see Table 1, so that 7.5° E in the left panel should be related to 10 ° E in the rigt panel for the coarse-fine transition.

to simulating eddy dynamics.

Any unstructured mesh with variable resolution contains geometrical irregularities in places where its resolution is changing, and local errors in representing numerical operators will more pronounced. Controlling these errors requires a certain level of mesh smoothness and the availability of dissipative operators that can handle the irregularities on the grid scale. For eddying flows, viscous dissipation is generally tuned so as to eliminate the cascade of variance at grid scales. On variable-resolution meshes this has an additional implication, for local dissipation has to eliminate the variance also in places where eddies are advected from the fine to coarse mesh, supplying variance at scales and with levels that do not match those of local dynamics. In practice this means that numerical stability and regular behavior of modeled fields need to be maintained, which of course depends on the discretization and simulated dynamics.

In all simulations reported here the dissipation (viscosity) is selected so as to maintain the grid-scale Reynolds number at a certain level when the mesh resolution is varied (h^3 scaling for biharmonic viscosities), and this turns out to be sufficient for preserving smooth behavior of temperature, velocity and relative vorticity, as illustrated by the snapshots in Fig. 1, and similar patterns in other simulations. With the exception of cases A′ and C′, the mesh transition occupies a zone which is just the size of a typical eddy, so that sharper transitions are hardly of practical interest. The ability of biharmonic operators to control the flow on such meshes is a very encouraging and important message. However, as is common in such situations, the full story is incomplete without analyzing the behavior of the vertical velocity (w). Inspection of w in case A (not shown) already reveals a noisy pattern at the fine-coarse transition (the coarse-fine transition remains virtually noise-free). Its presence indicates that either the available dissipation still fails to control all the details of solutions, or that some specific numerical issues come into play. The noise becomes stronger if the mesh resolution is refined. The upper panel of Fig. 8 presents a snapshot of vertical velocity from case E at approximately 400 m depth, where the problem of noise is much more apparent than in case A. In case E noise is seen in both transition zones, but is also present on the coarse mesh (around 35° E). We were not able to suppress the noise by increasing the viscosity threshold three-fold in the zones where the resolution is varied. However, we did not see any immediate effect of this noise on the model stability. There is no apparent increase in w-variance in places where it is present (it looks rather like scattering on mesh inhomogeneities).

The fact that noise is seen only in w, and not in the relative vorticity hints at the Hollingsworth instability (Hollingsworth et al. (1983)) which sometimes hampers the performance of codes based on the vector-invariant form of momentum advection and was explored for C-grid discretization. It should be recalled that the instability occurs because the two terms on the right hand side of the equality $(\mathbf{u}\cdot\nabla)\mathbf{u} = \omega\mathbf{e}_z\times\mathbf{u}+\nabla\mathbf{u}^2/2$, where $\mathbf{u}$ is the horizontal velocity and $\omega = (\nabla\times\mathbf{u})\cdot\mathbf{e}_z$ the relative vorticity, do not necessarily give the left hand side in the discrete formulation, but may contain an error that projects on the horizontal divergence and leads to instability. The problem does not occur for the relative vorticity because discretizations commonly maintain the property that the discrete curl operator gives exactly zero when applied to the discrete gradient. An analysis similar to the simplified analysis of Hollingsworth et al. (1983), however, shows that the cell-vertex (quasi-B-grid) discretization of the vector-invariant form of momentum employed by us is stable on uniform meshes, so that the problem can only be associated with some non-compensation on a variable mesh. While a rigorous analysis is beyond the scope of this paper (the eigenvalue analysis of Hollingsworth et al. (1983) can in principle be repeated on a limited patch of a non-uniform mesh), there are additional arguments in favor of this viewpoint.

In the upper panel of Fig. 8 there is no noise over the fine part, where the mesh is really uniform. Due to the mesh generation procedure, the coarse part is only quasi-uniform. This observation confirms that the noise is associated with mesh irregularity. Further, and more conclusive evidence is provided by the bottom panel of Fig. 8, showing a snapshot from simulations configured as case E except for the flux form of momentum advection. The noise is absent everywhere. The flux implementation of momentum advection is described by Danilov (2012). We first compute the flux divergence on scalar control volumes, and then average the result to vector points (cell centroids). Since the continuity is also formulated on scalar control volumes, this flux form is consistent with it.

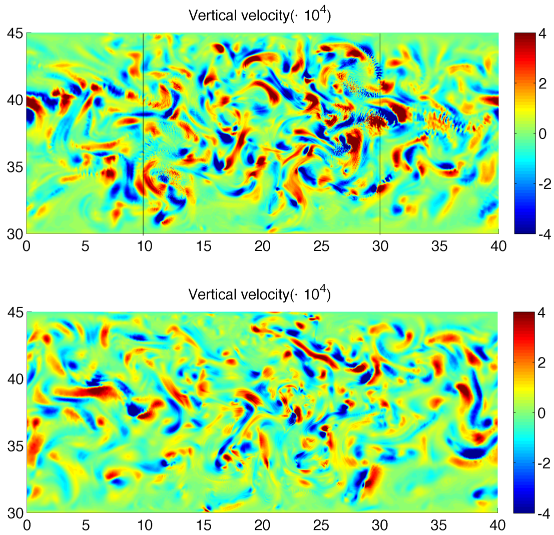

Figure 8: Snapshots of vertical velocity in case E at 400 m depth in simulations using the vector-invariant form (top) and the flux form (bottom) of momentum advection. Note the absence of noise in the second case and its presence in the first. The narrow transition zones are centered at the longitudes of 10° and 30° (indicated by black lines).

The flux form of momentum advection, eliminating the noise in w, also slightly modifies statistics as compared to the vector-invariant form, leading to lower values of variability for vertical velocity and relative vorticity. Since it does not change the response to the varied resolution we keep the simulations carried out with the vector-invariant form. The flux form of momentum advection can be discretized in many ways based on high-order transport schemes, but it remains to see how they behave in situations studied here.

4. Discussion

The question of how to refine the mesh resolution is a difficult one, and here we qualitatively explored only one of its aspects. The effect of retarded turbulence development has an implication that the area of refinement has to be sufficiently large or be connected through sufficiently wide transitional zones in order to "achieve" the goal resolution if the transition is made from a non-eddy-resolving mesh. Clearly, the examples considered above involve a particular flow and may to a degree overemphasize the effect. The dynamics are dominated by the zonal flow which advects transient features downstream leading to overshoots in variability as the flow passes from the fine to the coarse mesh, and retarded turbulence development when the flow passes from the coarse mesh to the fine mesh. The effect might be weaker for recirculation zones or marginal seas where the role of upstream 'seed' in triggering the development of turbulence will be less significant. It may also be reduced in the presence of small-scale topography triggering eddy formation. It remains to see whether this is so.

According to Hollingsworth et al. (1983) the noise in vertical velocity associated with the Hollingsworth instability depends on the detail of the implementation of the vector-invariant form of momentum advection. In our case, as mentioned above, the instability is not obtained on uniform meshes, and it is of interest to learn how it is linked to the mesh non-uniformity. It remains to see whether the vector-invariant form of momentum advection can be adjusted so as to eliminate the noise in the vertical velocity on highly-variable meshes, or whether it should be abandoned altogether on such meshes for the cell-vertex discretization. Although the behavior seen here is not necessarily characteristic of other unstructured-mesh discretizations, we think that the observation that the numerical implementation of momentum advection is of primary importance for maintaining smooth behavior of simulated fields on meshes with variable resolution is of general importance and deserves special attention on its own. We mention in this respect the analysis by Gassmann (2013) carried out for the quasi-hexagonal C-grid discretization which illustrates implications of the Hollingsworth instability and proposes measures to eliminate them on uniform meshes.

There are many related questions. Is the strategy to uniformly resolve the Rossby deformation radius in realistic applications a beneficial one? What is the optimal choice of switching from parameterized to resolved eddies on meshes with a strong change in resolution? The study of Hallberg (2013) suggests to sharply switch on/off the eddy parameterization where $L_R/h = 2$, and this may still be a good solution even in the presence of the retardation effect. Any continuation of thickness diffusion into the fine domain will further damp eddy motions there. And yet, the consequences of implementing this recommendation on meshes with strongly varying resolution remain to be explored. In addition, a local mesh refinement may modify the mean flow by virtue of the mean divergence of eddy Reynolds stresses. In simulations here the effects of this type were seen in deviation of the time-mean flow from strict zonality, induced by the mere change in the mesh resolution. Answering these questions would be of general interest. Indeed, since the Rossby radius varies substantially and becomes rather small at high latitudes, even current high-resolution ($1/10° - 1/12°$) models are on the edge between eddy-resolving and eddy-permitting over certain parts of the global ocean, facing similar questions. The impact of mesh refinement on the representation of eddy-topography interactions is yet another research topic, because many jets in the ocean are located in the vicinity of shelf break, where the Rossby radius varies substantially.

Although our study relies on unstructured meshes, situations where the mesh resolution is varied sharply occur in setups with nesting as well as on orthogonal curvilinear meshes where poles are taken close to each other to allow refinement in a particular region. The findings of this study should be in equal degree relevant in those cases too.

5. Conclusions

We show that changing the mesh resolution from coarse to eddy-resolving is accompanied by retardation in the turbulence saturation because of the absence of sufficiently strong perturbations in the flow upstream, which makes the effective geometrical resolution coarser. The effect is noticeable in zones about 10° wide in the test cases reported here when the coarse mesh is only eddy permitting. It becomes less significant if the coarse mesh is itself eddy resolving. The resolution of two mesh intervals per Rossby radius seems to define the boundary.

These statements have a qualitative character as the details may depend on applications. The presence of topography, details of domain geometry, or reduced velocity shear may modify the manifestation of the 'retardation' effect.

We also show that biharmonic viscosity operators with commonly used magnitude of biharmonic viscosity, scaled with the cube of the mesh size, are sufficient to ensure smoothness in the fields of temperature, horizontal velocity and relative vorticity even for sharp changes in the mesh resolution. However, changing the mesh resolution may lead to noise in the vertical velocity in the transition zones, which is linked to details of the vector-invariant momentum advection scheme, and is not present for the flux form of momentum advection.

Acknowledgments

We are indebted to anonymous reviewers for their suggestions and remarks.

References

Chanut, J., Barnier, B., Large, W., Debreu, L., Pendluff, T., Molines, J. M., Mathiot, P., 2008. Mesoscale eddies in the Labrador Sea and their contribution to convection and restratification, J. Phys. Oceanogr., 38, 1617–1643.

Danilov, S., 2012. Two finite-volume unstructured mesh models for large-scale ocean modeling. Ocean Model. 47, 1425. http://dx.doi.org/10.1016/j.ocemod.2012.01.004.

Danilov, S., Androsov, A., 2015. Cell-vertex discretization of shallow water equations on mixed unstructured meshes. Ocean Dynamics, 65, 33–47. DOI 10.1007/s10236-014-0790-x

Debreu, L., Blayo, E., 2008. Two-way embedding algorithms: a review. Ocean Dynamics, 58, 415–428.

Durgadoo, J. V., B. R. Loveday, C. J. C. Reason, P. Penven, and A. Biastoch, 2013. Agulhas leakage predominantly responds to the Southern Hemisphere westerlies. J. Phys. Oceanogr., 43, 2113–2131.

Fox-Kemper, B., Menemenlis, D., 2008. Can large eddy simulation techniques improve mesoscale rich ocean models? In: Hecht, M.W., Hasumi, H. (Eds.), 1679 Ocean Modeling in an Eddying Regime, Geophysical Monograph 177, AGU, pp. 1680 319337.

Gassmann, A., 2013. A global hexagonal C-grid non-hydrostatic dynamical core (ICON-IAP) designed for energetic consistency. Q.J.R. Meteorol. Soc. 139, 152-175.

Greenberg, D.A., Dupont, F., Lyard, F.H., Lynch, D.R., Werner, F.E., 2007. Resolution issues in numerical models of oceanic and coastal circulation. Cont. Shelf Res., 27, 13171343.

Hallberg, R., 2013. Using a resolution function to regulate parameterizations of oceanic mesoscale eddy effects. Ocean Modelling, 72, 92–103.

Hollingsworth, A., Kållberg, P., Renner, V. Burridge, D. M., 1983. An internal symmetric computational instability. Quart. J. R. Met. Soc., 109, 417–428.

Jansen, M. F., Held, I. M., 2014. Parameterizing subgrid-scale eddy effects using energetically consistent backscatter. Ocean Modelling, 80, 36–48.

Mertens, C., Rhein, M., Walter, M., Böning, C. W., Behrens, E., Kieke, D., Steinfeldt, R., Stöber, U., 2014. Circulation and transports in the Newfoundland Basin, western subpolar North Atlantic. J. Geophys. Res. - Oceans, 119, 7772–7793.

Pacanowski, R. C. and Philander, S. G. H., 1981. Parameterization of vertical mixing in numerical-models of tropical oceans. J. Phys. Oceanogr., 11, 14431451.

Ringler, T., Petersen, M., Higdon, R., Jacobsen, D., Maltrud, M., Jones, P.W., 2013. A multi-resolution approach to global ocean modelling. Ocean Model. Ocean Modelling, 69, 211–232.

Timmermann, R., Hellmer, H. H., 2013. Southern Ocean warming and increased ice shelf basal melting in the 21st and 22nd centuries based on coupled ice-ocean finite-element modelling, Ocean Dynamics, 63(9), 1011-1026, doi:10.1007/s10236-013-0642-0.

Wekerle, C., Wang, Q., Danilov, S., Jung, T., Schroter, J., 2013, The Canadian Arctic Archipelago throughflow in a multiresolution global model: Model assessment and the driving mechanism of interannual variability, J. Geophys. Res.: Oceans, doi:10.1002/jgrc.20330.